

Stepwise Bose-Einstein condensation in a spinor gas

C. Frapelli,¹ T. Zibold,^{1,*} A. Invernizzi,¹ K. Jiménez García,¹ J. Dalibard,¹ and F. Gerbier¹

¹*Laboratoire Kastler Brossel, Collège de France, CNRS, ENS-PSL Research University,
UPMC-Sorbonne Universités, 11 place Marcelin Berthelot, 75005 Paris*

(Dated: December 3, 2024)

We observe multi-step condensation of sodium atoms with spin $F = 1$, where the different Zeeman components $m_F = 0, \pm 1$ condense sequentially as the temperature decreases. The precise sequence changes drastically depending on the magnetization m_z , quadratic Zeeman energy q (QZE) in an applied magnetic field and interactions. For large QZE, the overall topology of the phase diagram is the same as for an ideal spin 1 gas, although the precise locations of the phase boundaries are significantly shifted by interactions. For small QZE, antiferromagnetic interactions qualitatively change the phase diagram, leading for instance to condensation in $m_F = \pm 1$, a phenomenon that would never occur for ideal gases with $q, m_z > 0$.

PACS numbers: 03.75.-b, 03.75.Hh

The properties of quantum fluids are often enriched by an internal degree of freedom. A historical example is liquid ^3He , where spin-triplet Cooper pairing leads to a richer phase diagram than the one of its spinless bosonic counterpart ^4He [1]. Spinor Bose-Einstein condensates [2–5], where several Zeeman components inside a given hyperfine spin F manifold are occupied, provide an atomic realization of multi-component quantum fluids. In such a system, spin-exchange collisions can redistribute populations among the Zeeman states [6–8], in contrast to other mixtures of quantum gases, *e.g.* those made with different species or with states belonging to different hyperfine manifolds.

An important property of spinor gases is the conservation of the longitudinal magnetization $m_z = \langle \hat{F}_z \rangle / N$ by short-range interatomic interactions driving the system to equilibrium. Here \hat{F} is the hyperfine spin operator and N the total atom number. This conservation law follows from the spin rotational symmetry of Van der Waals interactions when dipole-dipole interactions can be neglected [5]. The magnetization acts here as an external control parameter independent of the externally applied magnetic field B , in contrast with dipolar atoms [9] or with solid-state magnetic materials [10]. The linear Zeeman effect thus becomes irrelevant for the equilibrium state, since it is proportional to a conserved quantity. The main role of B is therefore to lower the energy of $m_F = 0$ with respect to $m_F = \pm 1$ by an amount $q \propto B^2$ (the quadratic Zeeman energy – QZE).

Depending on the value of F and on the strength of interactions, many low temperature magnetic phases with different spin order are possible in spinor gases [5]. In many cases, the spin order is determined by a competition between interactions and magnetic fields at very low energies, much less than typical thermal energies. Such low energy scales, negligible for normal gases, become relevant in presence of a condensate with macroscopic population. This mechanism (sometimes termed *Bose-enhanced magnetism* [5]) highlights the deep connection

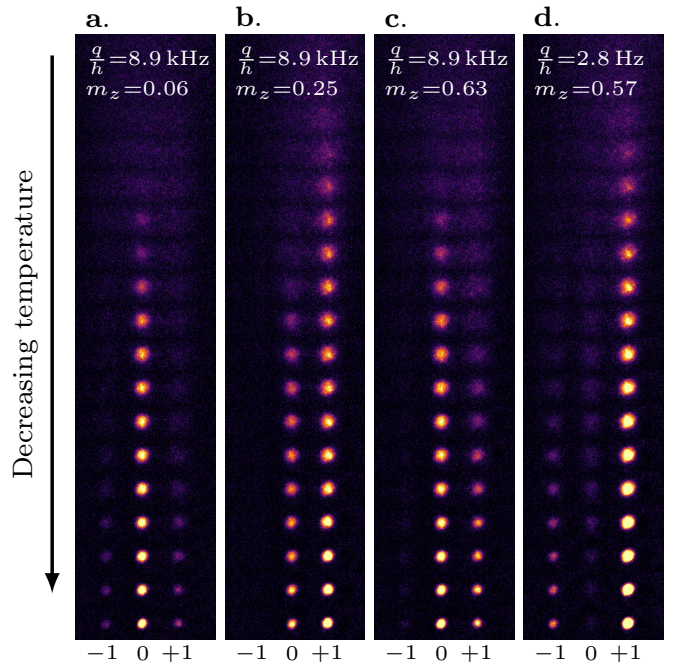


FIG. 1. Generic scenario for Bose-Einstein condensation in antiferromagnetic spin 1 gases. Each column is formed by juxtaposing absorption images of spin distributions with monotonically decreasing temperature T from top to bottom. The quadratic Zeeman energies and low- T magnetization m_z are indicated at the top of each column.

between Bose-Einstein condensation and magnetism in bosonic atomic gases, and raises the question of the stability of spin order against temperature.

In this letter, we report on an experimental study of the thermodynamic phase diagram of antiferromagnetic $F = 1$ condensates of sodium atoms. We observe that in general, Bose-Einstein condensation is established in steps when different Zeeman components condense one at a time. Fig. 1 shows four generic situations that occur when lowering the temperature starting from a normal

Bose gas. Without loss of generality, we focus in this work on the case of positive magnetization, given that the case of $m_z < 0$ can be deduced by symmetry. For large QZE and vanishing magnetization $m_z \approx 0$, Fig. 1 a shows that only the $m_F = 0$ component condenses ($m_F = 0, \pm 1$ are the three Zeeman states). In all cases with $m_z \neq 0$, we find a sequence of transitions where different Zeeman components condense at different temperatures, either $m_F = +1$ first and $m_F = 0$ second for high magnetizations (Fig 1 b) or the reverse situation for lower magnetizations (Fig 1 c). For small QZE instead, the condensate first forms in $m_F = +1$ and second in $m_F = -1$, while $m_F = 0$ does not condense for the magnetization in Fig. 1 d. The purpose of this paper is to explore the rich landscape of transitions in a bosonic spinor system and to elucidate the role of the QZE and atomic interactions.

The present work is to the best of our knowledge the first comprehensive measurement of thermodynamic properties of spinor condensates with conserved magnetization. Previous experimental works exploring finite temperatures in spinor gases studied spin dynamics in thermal gases [11, 12], dynamical formation of condensates after quenches [13, 14], and demonstrated cooling of the majority Zeeman component by selective evaporation of the minority components [15, 16]. The realization of dipolar spinor gases with free magnetization [9] was limited to the study of spin-polarized condensed phases in equilibrium due to dipolar relaxation. More recently, a gas of spin excitations in a spin-polarized ($m_z \approx 1$) ferromagnetic Bose-Einstein condensate was observed to equilibrate and even condense at sufficiently low temperatures [17].

In contrast to the sparse experimental literature, thermodynamics of spinor gases has been extensively studied theoretically using various assumptions and methods. The ideal spin 1 gas has been discussed in Refs. [18, 19] for $q = 0$, and in Ref. [20] for $q \neq 0$. The role of interactions has been explored using various approximations [18, 21–24]. However, our experimental results can be fully understood only when taking into account three important features, the harmonic trap (which is crucial to stabilize an antiferromagnetic condensate in a single spatial mode [25]), the QZE and the interactions.

Our experiments are performed with a cloud of ultracold ^{23}Na atoms in a crossed optical dipole trap (ODT). The three experimental control parameters are the QZE q , the magnetization m_z and the trap depth V_0 . The longitudinal magnetization m_z is set by a preparation sequence performed far above T_c , allowing us to vary between unmagnetized samples ($m_z \approx 0$) and fully magnetized samples ($m_z \approx 1$) (see [26, 27]). The trap depth V_0 controls the evaporative cooling trajectory leading to quantum degeneracy, the temperature T and total atom number N . The ODT is tight enough such that a condensate forms in the so-called single-mode regime [25], where the spatial shape of the condensate wavefunction

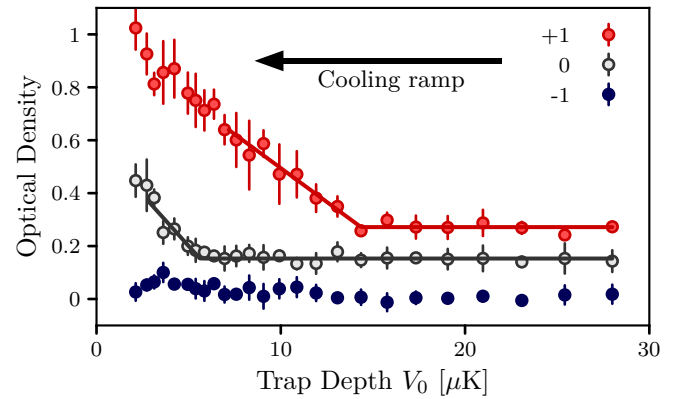


FIG. 2. Evolution of peak optical density with trap depth for a particular evaporation trajectory with $q/h \approx 69$ Hz and $m_z \approx 0.3$ at the highest temperature. For these parameters, the $m_F = +1$ component condenses first (at a temperature $T_{c,1} \approx 1.8 \mu\text{K}$), followed by the $m_F = 0$ component (at a temperature $T_{c,2} \approx 560 \text{nK}$). No condensate was detected in the $m_F = -1$ component. The curves for $m_F = +1$ and $m_F = 0$ have been shifted vertically by 0.2 and 0.1 for clarity. The error bars denote statistical uncertainties at a 66 % confidence level. The solid lines indicate the piece-wise linear fits used to determine the critical trap depths.

is independent of the Zeeman state. In the following, we characterize our data at a given value of q, m_z by an evaporation “trajectory” (N, T), taking four experimental realizations for each point in the trajectory.

Absorption images as shown in Fig. 1 are recorded after 3 ms of expansion in an applied magnetic field gradient [27]. We perform a fit to a bimodal distribution for each component to extract the atom number N_{m_F} and condensed fraction f_{c,m_F} per component as well as the total atom number N . We determine the temperature of the thermal part from fits to the wings of the distribution [27]. We found that the condensed fraction obtained from the fits was not suitable to determine the critical temperature. Indeed, low condensed fractions $< 5\%$ are difficult to detect with the fit algorithm due to a combination of low signal-to-noise ratio and the complexity of fitting the three Zeeman components simultaneously.

The signature of BEC is the appearance of a dense, narrow peak near the center of the atomic distribution. The onset of BEC can be tracked by monitoring the peak optical density (OD), taken as a proxy for the condensed fraction [28]. Measurements of the peak OD avoid relying on bimodal fits or other indirect analyses with uncontrolled systematic biases. Fig. 2 shows such a measurement for a particular evaporation trajectory. The peak OD increases sharply when Bose-Einstein condensation is reached. In this example, we demonstrate a two-step condensation as predicted in [18] for an ideal spin 1 gas, where the $m_F = +1$ component condenses first, followed by the $m_F = 0$ component. For a given evaporation trajectory, we identify the critical trap depth $V_{0,c}$ where

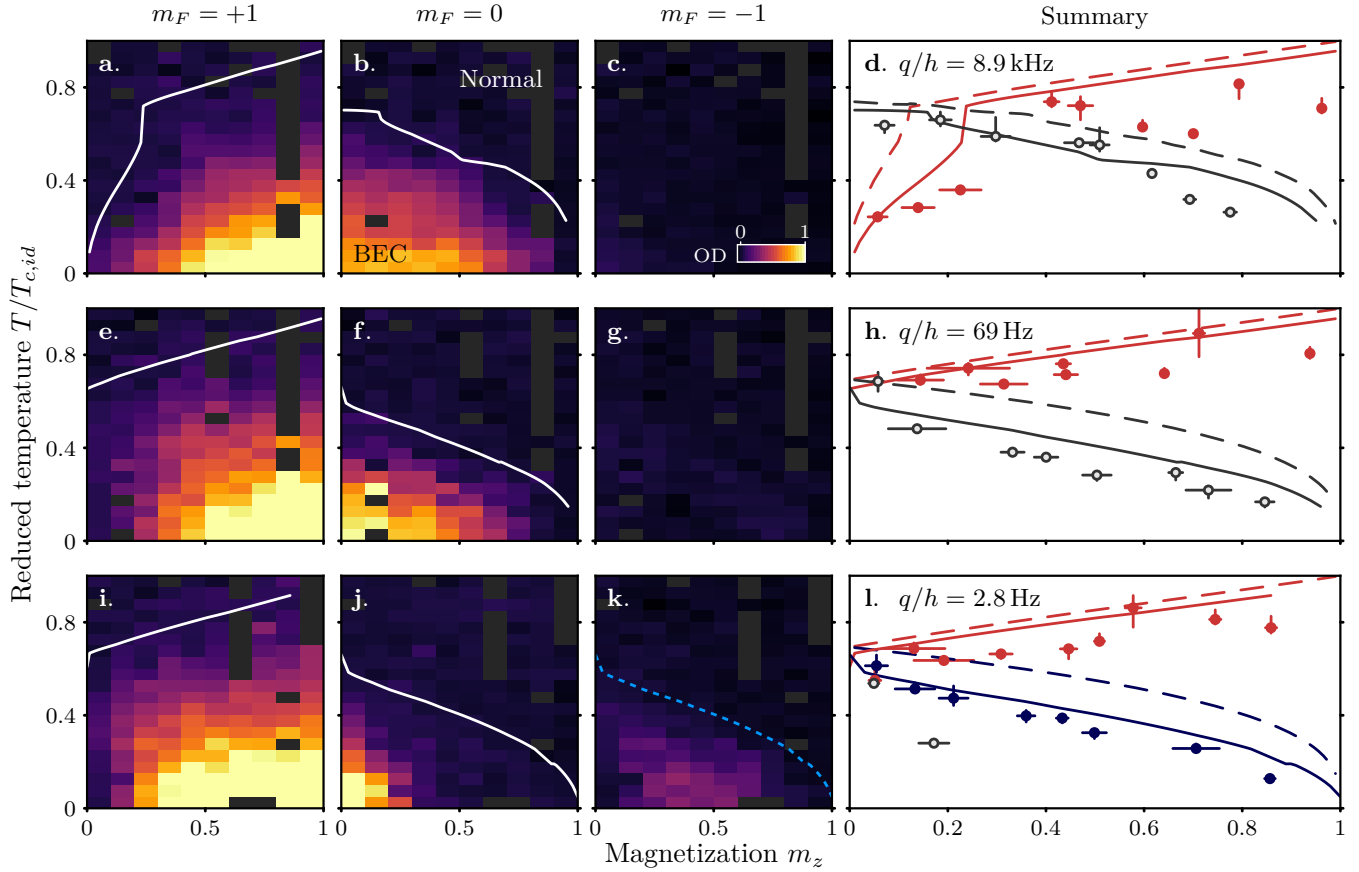


FIG. 3. Thermodynamic phase diagram of an antiferromagnetic spin $F = 1$ Bose gas. The peak optical density of each Zeeman component is reported for the entire set of data at each value of the QZE $-q/h = 8.9$ kHz (a-c), 69 Hz (e-g) and $q = 2.8$ Hz (i-k). The temperature is normalized to $T_{c,id}$, the critical temperature of a *single-component* ideal Bose gas with the same number of atoms. The grayed areas indicate the absence of data in the corresponding regions. The right column (d,h,l) shows the measured critical temperatures of the $m_F = +1, 0, -1$ Zeeman components (red, gray, and dark blue markers, respectively). The solid (dashed) lines are the predictions of an Hartree-Fock model with spin-independent interactions (ideal gas theory). The dotted line in k shows the expected $T_{c,2}$ where $m_F = 0$ condenses according to the Hartree-Fock model.

condensation is reached by a piece-wise linear fit to the data, taking the intercept point as the experimentally determined $V_{0,c}$ (see Fig. 2). We interpolate numerically the atom number, magnetization and temperature to obtain the critical values N_c , T_c , $m_{z,c}$ from $V_{0,c}$.

Fig. 3 summarizes the results of this work. We show the peak optical density for each Zeeman component and each value of q in a $(T - m_z)$ plane (Fig. 3 a-c, e-g and i-k). In this plot, all data taken at a given QZE q are binned with respect to magnetization and temperature. The domains where condensation occurs appear in light colors. For convenience, the temperature is scaled to the critical temperature of a *single-component* ideal gas $k_B T_{c,id} = \hbar \bar{\omega} [N/\zeta(3)]^{1/3}$, with $\bar{\omega}$ the geometric average of the trap frequencies and ζ the Riemann zeta function [29]. The same plot also shows the measured critical temperatures (Fig. 3 d, h, l). In one case, $m_F = 0$ when $m_z \approx 0.3$ and $q/h = 2.8$ Hz, the lowest temperature images do show a condensed component but the critical

temperature could not be extracted reliably from the fitting procedure due to sparse sampling. This particular point is not reported in Fig. 3l. The phenomenon of sequential condensation is always observed for $m_z \neq 0$, but the overall behavior changes drastically with q .

We first discuss the cases with largest QZE, $q/h \approx 8.9$ kHz (Fig. 3 a-d) and $q/h \approx 69$ Hz (Fig. 3 e-h). The last case with small $q/h \approx 3$ Hz will be discussed later. For $q/h \approx 8.9$ kHz and highly magnetized samples (as in Fig. 2), the majority component $m_F = +1$ condenses first at a critical temperature $T_{c,1}$, followed by the $m_F = 0$ component at a lower temperature $T_{c,2}$. For low magnetizations, the condensation sequence is reversed : $T_{c,1}$ corresponds to condensation of the $m_F = 0$ component and $T_{c,2}$ to $m_F = +1$. For $q/h \approx 69$ Hz, we observe only one sequence, a two-step condensation with $m_F = +1$ first and $m_F = 0$ second.

Sequential condensation of a spin 1 Bose gas is expected on the basis of the ideal gas theory when the QZE

and the conservation of magnetization are taken into account [20]. For an ideal single-component gas, Bose-Einstein condensation occurs when the chemical potential of the gas becomes equal to the energy of the lowest single-particle state [29]. For a spin 1 gas, the same criterion holds but with modified state-dependent chemical potentials $\mu_0 = \mu$ and $\mu_{\pm 1} = \mu \pm \lambda$, where λ is a Lagrange multiplier introduced to account for the conservation of m_z . For $m_z = 0$ ($\lambda = 0$) and $q > 0$, the QZE lowers the energy of the $m_F = 0$ state, which is therefore the first component to condense when $\mu = -q$. For $m_z > 0$, λ is positive and increases with m_z . The energetic advantage of $m_F = 0$ is in balance with the statistical trend favoring the most populated component $m_F = +1$. Eventually, this trend takes over at a “critical” value m_z^* (where $\lambda = q$). For $m_z > m_z^*$, the $m_F = +1$ component becomes the first to condense.

Figure 3d-h shows the measured critical temperatures and compares them to the prediction of the ideal gas theory. We observe a systematic shift of $T_{c,1}$ and $T_{c,2}$ towards lower temperatures. The shift of $T_{c,1}$ is small, and could be an artifact due to the difficulty to detect small condensate fractions of a few percents. However, the shift of $T_{c,2}$ is too large to be explained by the same reason. We also find an experimental “critical” value $m_z^* \sim 0.22$ larger than the one expected for an ideal gas. The behavior for $q/h \approx 69$ Hz (Fig. 3e-h) is qualitatively similar to the largest q case, but with a small critical value m_z^* that cannot be resolved experimentally (the ideal gas theory predicts ≈ 0.002).

For single-component gases, repulsive interactions lower the critical temperature [30]. The same effect can be expected to occur for a spinor gas, with an enhanced shift of $T_{c,2}$ due to the presence of a condensate. To substantiate these qualitative observations and to obtain a quantitative prediction for a spinor gas, we use a simplified version of Hartree-Fock theory [24]. Our self-consistent calculations include the trap potential in a semi-classical approximation, and treat the interactions as spin-independent. These approximations are valid only above $T_{c,2}$, where at most one component condenses [27]. The calculations are performed for atom numbers and trap frequencies matching the experimental values at the observed transition points [27].

The results of the self-consistent Hartree-Fock calculation are shown in Figure 3d-i, and qualitatively account for the experimental data. They explain in particular the strong downwards shift of $T_{c,2}$ for all q and the shift of m_z^* to higher values for $q/h \approx 8.9$ kHz. A noticeable feature for $q/h \approx 8.9$ kHz is a “jump” of $T_{c,2}$ when crossing m_z^* from left to right, which is present in the calculation and in the data [27]. A residual downwards shift of 7–8% remains. It could be partially explained by finite-size and trap anharmonicity effects, which are not included in the Hartree-Fock calculation [27].

At the lowest field we studied, $q/h \approx 2.8$ Hz (Fig. 3i

l), we observe a change in the *nature* of $T_{c,2}$. For high values of m_z , $T_{c,2}$ corresponds to condensation into the $m_F = -1$ state while the $m_F = 0$ component remains uncondensed. This phenomenon is incompatible with ideal gas theory *and* with our Hartree-Fock model with spin-independent interactions, where the $m_F = -1$ component never condenses for $q > 0$ [18, 20]. It corresponds to a change of the magnetic ordering appearing below $T_{c,2}$. Coexisting $m_F = 0$ and $m_F = +1$ components with a well-defined phase relation correspond to a spinor condensate with non-zero values of the longitudinal $\langle \hat{S}_z \rangle = m_z$ and of the transverse spin $\langle \hat{S}_x + i\hat{S}_y \rangle \neq 0$ (the so-called “broken axisymmetry” phase) [5]. In contrast, coexisting $m_F = \pm 1$ components correspond to a spin-nematic phase, where $\langle \hat{S}_z \rangle = m_z$ but $\langle \hat{S}_x + i\hat{S}_y \rangle = 0$ [5]. This change in the magnetic properties of antiferromagnetic spinor condensates has been observed previously at very low temperatures [26, 31–34].

At $T = 0$ and in the single-mode regime, the transition occurs for $q < U_s$ at a critical magnetization $m_{z,c} = \sqrt{1 - [1 - (q/U_s)]^2}$, with U_s a spin-dependent interaction energy [35]. For the coldest clouds at $q/h = 2.8$ Hz, we estimate [26] $U_s/h \lesssim 50$ Hz and $m_{z,c} \gtrsim 0.3$, in fair agreement with Fig. 3j-k. When $q > U_s$, there is no phase transition and only the broken axisymmetry phase is present. This explains the qualitative difference between the data for $q/h = 2.8$ Hz and for the other two values.

The experimental data in Fig. 3l indicate that the region of the phase diagram occupied by the broken axisymmetry phase at the lowest q shrinks with increasing temperature. In fact, we find that $m_F = -1$ condenses at $T_{c,2}$ for all parameters we have explored, with $m_F = 0$ eventually condensing at a third critical temperature (except for very low m_z , where all components appear to condense together within the accuracy of our measurement). The dashed line in Fig. 3k shows $T_{c,2}$ predicted by the Hartree-Fock model with spin-independent interactions. Although the model incorrectly predicts that $m_F = 0$ should condense below $T_{c,2}$, the predicted transition closely matches the observed boundary between single-component $m_F = +1$ BEC and spin nematic $m_F = \pm 1$ BEC. This indicates that the transition line itself (but not the magnetic order below it) is determined by the thermal component alone.

In conclusion, we have studied the thermodynamics of spin 1 Bose gases with antiferromagnetic interactions. For condensates in the single-mode regime, we observed a sequence of transitions for each Zeeman component. For high QZE, only two component condense favored by the imposed magnetization and the QZE. For low QZE ($q/h = 2.8$ Hz), we find three condensation transitions, the lower two leading to different magnetic order. We have found quantitative agreement between the measured change of the critical temperatures $T_{c,1}$ and $T_{c,2}$ with magnetization and a self-consistent Hartree-Fock model. However, this model is limited to temperatures above $T_{c,2}$

and cannot make any prediction for the low-temperature behavior at low QZE. Indeed, the model assumes that only a single-component condensate is present and that spin-dependent interactions can be neglected. Both assumptions are clearly invalid. A more complete theoretical analysis accounting for all experimental results and elucidating the exact nature of the low-temperature transitions for low QZE remains an open problem.

We acknowledge stimulating discussions with B. Evrard, L. De Sarlo, E. Witkowska, J. Beugnon, L. de Forges de Parny, A. Rançon and T. Roscilde. This work has been supported by the EU (ERC Synergy grant UQUAM). TZ acknowledges funding from the Hamburg Center for Ultrafast Imaging, and KJG from the European Union's Horizon 2020 research and innovation programme under the Marie Skłodowska-Curie grant agreement No. 701894.

* Current address: Department of Physics, University of Basel, Klingelbergstrasse 82, 4056 Basel, Switzerland

- [1] D. Vollhardt and P. Wölfle, *The Superfluid Phases of Helium 3* (Taylor and Francis, London, 1990).
- [2] T.-L. Ho, “Spinor Bose condensates in optical traps,” *Phys. Rev. Lett.* **81**, 742–745 (1998).
- [3] T. Ohmi and K. Machida, “Bose-Einstein condensation with internal degrees of freedom in alkali atom gases,” *Journal of the Physical Society of Japan* **67**, 1822–1825 (1998).
- [4] J. Stenger, S. Inouye, D. Stamper-Kurn, H.-J. Miesner, A. Chikkatur, and W. Ketterle, “Spin domains in ground-state Bose-Einstein condensates,” *Nature* **396**, 345–348 (1998).
- [5] D. M. Stamper-Kurn and M. Ueda, “Spinor Bose gases: Symmetries, magnetism, and quantum dynamics,” *Rev. Mod. Phys.* **85**, 1191–1244 (2013).
- [6] M.-S. Chang, C. D. Hamley, M. D. Barrett, J. A. Sauer, K. M. Fortier, W. Zhang, L. You, and M. S. Chapman, “Observation of spinor dynamics in optically trapped ^{87}Rb Bose-Einstein condensates,” *Phys. Rev. Lett.* **92**, 140403 (2004).
- [7] H. Schmaljohann, M. Erhard, J. Kronjäger, M. Kottke, S. van Staa, L. Cacciapuoti, J. J. Arlt, K. Bongs, and K. Sengstock, “Dynamics of $F = 2$ spinor Bose-Einstein condensates,” *Phys. Rev. Lett.* **92**, 040402 (2004).
- [8] T. Kuwamoto, K. Araki, T. Eno, and T. Hirano, “Magnetic field dependence of the dynamics of ^{87}Rb spin-2 Bose-Einstein condensates,” *Phys. Rev. A* **69**, 063604 (2004).
- [9] B. Pasquiou, E. Maréchal, L. Vernac, O. Gorceix, and B. Laburthe-Tolra, “Thermodynamics of a Bose-Einstein condensate with free magnetization,” *Phys. Rev. Lett.* **108**, 045307 (2012).
- [10] L.-P. Levy, *Magnetism and Superconductivity* (Springer, Berlin, 2000).
- [11] H. K. Pechkis, J. P. Wrubel, A. Schwettmann, P. F. Griffin, R. Barnett, E. Tiesinga, and P. D. Lett, “Spinor dynamics in an antiferromagnetic spin-1 thermal Bose gas,” *Phys. Rev. Lett.* **111**, 025301 (2013).
- [12] X. He, B. Zhu, X. Li, F. Wang, Z.-F. Xu, and D. Wang, “Coherent spin-mixing dynamics in thermal ^{87}Rb spin-1 and spin-2 gases,” *Phys. Rev. A* **91**, 033635 (2015).
- [13] M. Erhard, H. Schmaljohann, J. Kronjäger, K. Bongs, and K. Sengstock, “Bose-Einstein condensation at constant temperature,” *Phys. Rev. A* **70**, 031602 (2004).
- [14] B. Naylor, M. Brewczyk, M. Gajda, O. Gorceix, E. Maréchal, L. Vernac, and B. Laburthe-Tolra, “Competition between Bose-Einstein condensation and spin dynamics,” *Phys. Rev. Lett.* **117**, 185302 (2016).
- [15] R. Olf, F. Fang, G. E. Marti, A. MacRae, and D. M. Stamper-Kurn, “Thermometry and cooling of a Bose gas to 0.02 times the condensation temperature,” *Nat. Phys.* **11**, 720–723 (2015).
- [16] B. Naylor, E. Maréchal, J. Huckans, O. Gorceix, P. Pedri, L. Vernac, and B. Laburthe-Tolra, “Cooling of a Bose-Einstein condensate by spin distillation,” *Phys. Rev. Lett.* **115**, 243002 (2015).
- [17] F. Fang, R. Olf, S. Wu, H. Kadau, and D. M. Stamper-Kurn, “Condensing magnons in a degenerate ferromagnetic spinor Bose gas,” *Phys. Rev. Lett.* **116**, 095301 (2016).
- [18] T. Isoshima, T. Ohmi, and K. Machida, “Double phase transitions in magnetized spinor Bose-Einstein condensation,” *Journal of the Physical Society of Japan* **69**, 3864–3869 (2000).
- [19] Kao, Y.-M. and Jiang, T. F., “Transition temperatures of the trapped ideal spinor Bose gas,” *Eur. Phys. J. D* **40**, 263–269 (2006).
- [20] G. Lang and E. Witkowska, “Thermodynamics of a spin-1 Bose gas with fixed magnetization,” *Phys. Rev. A* **90**, 043609 (2014).
- [21] W. Zhang, S. Yi, and L. You, “Bose-Einstein condensation of trapped interacting spin-1 atoms,” *Phys. Rev. A* **70**, 043611 (2004).
- [22] S. Uchino, M. Kobayashi, and M. Ueda, “Bogoliubov theory and Lee-Huang-Yang corrections in spin-1 and spin-2 Bose-Einstein condensates in the presence of the quadratic Zeeman effect,” *Phys. Rev. A* **81**, 063632 (2010).
- [23] N. T. Phuc, Y. Kawaguchi, and M. Ueda, “Effects of thermal and quantum fluctuations on the phase diagram of a spin-1 ^{87}Rb Bose-Einstein condensate,” *Phys. Rev. A* **84**, 043645 (2011).
- [24] Y. Kawaguchi, N. T. Phuc, and P. B. Blakie, “Finite-temperature phase diagram of a spin-1 Bose gas,” *Phys. Rev. A* **85**, 053611 (2012).
- [25] S. Yi, Ö. E. Müstecaplıoğlu, C. P. Sun, and L. You, “Single-mode approximation in a spinor-1 atomic condensate,” *Phys. Rev. A* **66**, 011601 (2002).
- [26] D. Jacob, L. Shao, V. Corre, T. Zibold, L. De Sarlo, E. Mimoun, J. Dalibard, and F. Gerbier, “Phase diagram of spin-1 antiferromagnetic Bose-Einstein condensates,” *Phys. Rev. A* **86**, 061601 (2012).
- [27] (See Supplemental Material at [URL will be inserted by publisher]).
- [28] S. Trotzky, L. Pollet, F. Gerbier, U. Schnorrberger, I. Bloch, M. Troyer, N. V. Prokof'ev, and B. V. Svistunov, “Suppression of the critical temperature for superfluidity near the Mott transition,” *Nat. Phys.* **6**, 998–1004 (2010).
- [29] F. Dalfovo, S. Giorgini, L. P. Pitaevskii, and S. Stringari, “Theory of Bose-Einstein condensation in trapped

gases,” *Rev. Mod. Phys.* **71**, 463–512 (1999).

[30] S. Giorgini, L. P. Pitaevskii, and S. Stringari, “Condensate fraction and critical temperature of a trapped interacting Bose gas,” *Phys. Rev. A* **54**, R4633–R4636 (1996).

[31] Y. Liu, S. Jung, S. E. Maxwell, L. D. Turner, E. Tiesinga, and P. D. Lett, “Quantum phase transitions and continuous observation of spinor dynamics in an antiferromagnetic condensate,” *Phys. Rev. Lett.* **102**, 125301 (2009).

[32] A. Vinit, E. M. Bookjans, C. A. R. Sá de Melo, and C. Raman, “Antiferromagnetic spatial ordering in a quenched one-dimensional spinor gas,” *Phys. Rev. Lett.* **110**, 165301 (2013).

[33] J. Jiang, L. Zhao, M. Webb, and Y. Liu, “Mapping the phase diagram of spinor condensates via adiabatic quantum phase transitions,” *Phys. Rev. A* **90**, 023610 (2014).

[34] L. Zhao, J. Jiang, T. Tang, M. Webb, and Y. Liu, “Antiferromagnetic spinor condensates in a two-dimensional optical lattice,” *Phys. Rev. Lett.* **114**, 225302 (2015).

[35] W. Zhang, S. Yi, and L. You, “Mean field ground state of a spin-1 condensate in a magnetic field,” *New Journal of Physics* **5**, 77 (2003).